
CIN++: Enhancing Topological Message Passing

Lorenzo Giusti*
Sapienza University
lorenzo.giusti@uniroma1.it

Teodora Reu
University of Cambridge
tr500@cam.ac.uk

Francesco Ceccarelli
University of Cambridge
fc485@cam.ac.uk

Cristian Bodnar
Microsoft Research AI4Science
cbodnar@microsoft.com

Pietro Liò
University of Cambridge
p1219@cam.ac.uk

Abstract

Graph Neural Networks (GNNs) have demonstrated remarkable success in learning from graph-structured data. However, they face significant limitations in expressive power, struggling with long-range interactions and lacking a principled approach to modeling higher-order structures and group interactions. Cellular Isomorphism Networks (CINs) recently addressed most of these challenges with a message passing scheme based on cell complexes. Despite their advantages, CINs make use only of boundary and upper messages which do not consider a direct interaction between the rings present in the underlying complex. Accounting for these interactions might be crucial for learning representations of many real-world complex phenomena such as the dynamics of supramolecular assemblies, neural activity within the brain, and gene regulation processes. In this work, we propose CIN++, an enhancement of the topological message passing scheme introduced in CINs. Our message passing scheme accounts for the aforementioned limitations by letting the cells to receive also lower messages within each layer. By providing a more comprehensive representation of higher-order and long-range interactions, our enhanced topological message passing² scheme achieves state-of-the-art results on large-scale and long-range chemistry benchmarks.

1 Introduction

Graph Neural Networks (GNNs) find applications in a plethora of fields, like computational chemistry [1], social networks [2] and physics simulations [3]. Since their introduction [4, 5], GNNs have shown remarkable results in learning tasks when data are defined over a graph domain, where the flexibility of neural networks is coupled with prior knowledge about data relationships, expressed in terms of the underlying topology [6]. The idea behind GNNs is learning representations of node features using local aggregation, where the neighbourhood is formally represented by the underlying graph, which can be seen as a simple instance of a *topological space*, able to capture *pairwise* interactions through the presence of an edge between any pair of directly interacting nodes. By leveraging this simple but powerful idea, outstanding performance has been achieved in many traditional tasks such as classification for nodes or entire graphs [7] or link prediction [8] as well as more specialized ones such as *protein folding* [9] and *algorithmic reasoning* [10]. While Graph Neural Networks (GNNs) have advanced the modelling of pairwise interactions on graph-structured data, their inability to accurately capture long-range and group interactions, along with their struggles to manage higher-order structures, are significant shortcomings. These limitations critically restrict the application of GNNs in understanding real-world complex systems.

*The work was performed while the author was in Cambridge.

²The code implementation can be found at: <https://github.com/twitter-research/cwn>

	$\mathcal{B}(\sigma)$	$\mathcal{Co}(\sigma)$	$\mathcal{N}^+(\sigma)$	$\mathcal{N}^-(\sigma)$
$\sigma \in \mathcal{V}$	\emptyset			\emptyset
$\sigma \in \mathcal{E}$				
$\sigma \in \mathcal{R}$		\emptyset	\emptyset	

Figure 1: Visual representation of adjacencies within cell complexes. The reference cell, σ , is showcased in blue, with adjacent cells τ highlighted in green. Any intermediary cells, δ , facilitating connectivity are depicted in yellow.

To cope with these limitations, a major performance boost to GNNs algorithms has been offered by considering more complex topological spaces such as simplicial complexes [11] or cell complexes [12], introduced to handle tasks for data that are naturally defined on higher-order elements. Then, these ideas were combined with provably powerful message-passing schemes on simplicial [13] and cell complexes [14] achieving remarkable results. Nonetheless, the aforementioned models are unable to discover consistently long-range and group interactions, which play a crucial role in many practical applications such as network neuroscience [15], physics of complex systems [16] or gene regulatory networks [17], where some reactions occur only when a group of more than two entities interact.

Contribution In this work, we leverage the advantages of complex topological spaces to introduce a novel message-passing scheme on cell complexes. Motivated by the fact that cell complexes provide a natural framework to represent higher-dimensional structures and topological features that are inherent in the realm of chemistry, throughout this work, we will mostly focus on this domain. In particular, we enhanced the Topological Message Passing scheme defined in [14] by including messages that flow within the lower neighbourhood of the underlying cell complex. These are messages exchanged between edges that share a common vertex and between rings that are glued through an edge to better capture group interactions and escape potential bottlenecks. In the experimental section, we show that with respect to other models, this representation allows for a more natural and comprehensive understanding of chemical systems and their properties, resulting in state-of-the-art performance in both a large-scale molecular benchmark (ZINC) and a long-range graph benchmark (Peptides). We see that the ability of our model to understand higher-dimensional structures and topological features could have an immediate and significant impact in the areas of computational chemistry and drug discovery.

2 Background

In this section, we recall the basics of regular cell complexes. These are topological spaces that enable efficient representation of high-order interaction systems, generalizing graphs and simplicial complexes. In particular, we first introduce the definition of a regular cell complex and then we recall a few additional properties enabling the representation of cell complexes via boundary operators.

Definition 1 (Regular Cell Complex). [18] *A regular cell complex is a topological space \mathcal{C} together with a partition $\{\mathcal{C}_\sigma\}_{\sigma \in \mathcal{P}_\mathcal{C}}$ of subspaces \mathcal{C}_σ of \mathcal{C} called cells, where $\mathcal{P}_\mathcal{C}$ is the indexing set of \mathcal{C} , such that*

1. For each $\sigma \in \mathcal{C}$, every sufficient small neighbourhood of σ intersects finitely many \mathcal{C}_σ ;
2. For all τ, σ we have that $\mathcal{C}_\tau \cap \bar{\mathcal{C}}_\sigma \neq \emptyset$ iff $\mathcal{C}_\tau \subseteq \bar{\mathcal{C}}_\sigma$, where $\bar{\mathcal{C}}_\sigma$ is the closure of the cell;
3. Every \mathcal{C}_σ is homeomorphic to \mathbb{R}^k for some k ;
4. For every $\sigma \in \mathcal{P}_\mathcal{C}$ there is a homeomorphism ϕ of a closed ball in \mathbb{R}^k to $\bar{\mathcal{C}}_\sigma$ such that the restriction of ϕ to the interior of the ball is a homeomorphism onto \mathcal{C}_σ .

Condition 2 implies that the indexing set \mathcal{P}_C has a poset structure, given by $\tau \leq \sigma$ iff $\mathcal{C}_\tau \subseteq \overline{\mathcal{C}_\sigma}$. This is known as the face poset of \mathcal{C} . The regularity condition (4) implies that all topological information about \mathcal{C} is encoded in the poset structure of \mathcal{P}_C . Then, a regular cell complex can be identified with its face poset. For this reason, from now on we will indicate the cell \mathcal{C}_σ with its corresponding face poset element σ which dimension $\dim(\sigma)$ is equal to the dimension of the space homeomorphic to \mathcal{C}_σ . In this study, we focus on cell complexes with cells of maximum dimension equal to 2.

In this context, a graph $\mathcal{G} = (\mathcal{V}, \mathcal{E})$ can be viewed as a particular case of a regular cell complex \mathcal{C} . Specifically, a graph is a cell complex where the set of 2-cells is the empty set. In this context, the vertices of the graph correspond to the 0-cells in \mathcal{C} , while the edges of the graph are then represented by its 1-cells, connecting pairs of vertices. Throughout this work, we will consider regular cell complexes \mathcal{C} built using *skeleton-preserving cellular lifting maps* [14] from an input graph \mathcal{G} . A pictorial example of this operation is provided in Fig. 2, where filled rings are attached to closed paths of edges having no internal chords.

Definition 2 (Boundary Relation). *Given two cells $\sigma, \tau \in \mathcal{C}$. We have the boundary relation $\sigma \triangleleft \tau$ iff $\dim(\sigma) \leq \dim(\tau)$ and $\nexists \delta \in \mathcal{C} : \sigma \triangleleft \delta \triangleleft \tau$.*

We can leverage the previous definitions to characterize the different types of neighbourhoods present in cell complexes.

Boundary Neighbourhood For a cell σ , the boundary is a set $\mathcal{B}(\sigma) = \{\tau \mid \tau \triangleleft \sigma\}$ composed by the lower-dimensional cells that respect Definition 2. In the first column of Fig. 1 we depicted a glossary of the boundary neighbourhoods of a regular cell complex \mathcal{C} . In particular, a vertex does not have a boundary neighbourhood, an edge has a boundary composed of the nodes attached to its endpoints, while the boundary cells of a ring are the edges that enclose the ring itself.

Co-Boundary Neighbourhood For a cell σ , the co-boundary neighbourhood is a set $\mathcal{Co}(\sigma) = \{\tau \mid \sigma \triangleleft \tau\}$ of higher-dimensional cells with σ on their boundary. For a node, its co-boundary is composed of the edges that have that node as an endpoint. For an edge, it is the set of rings that have that edge as one of their sides. In our case, rings do not have a co-boundary neighbourhood. We show a pictorial example of the various co-boundary neighbourhoods in the second column of Fig. 1.

Upper Neighbourhood These are the cells of the same dimension as σ that are on the boundary of the same higher-dimensional cell as σ : $\mathcal{N}^\uparrow(\sigma) = \{\tau \mid \exists \delta : \sigma \triangleleft \delta \wedge \tau \triangleleft \delta\}$. For instance, as shown in the third column of Fig. 1, the upper adjacent cells of a vertex v_i are the vertices connected to v_i via an edge (i.e., the canonical graph adjacency). The upper adjacent cells of an edge e_i are the edges that surround the rings for which e_i is a boundary element. However, in a 2-Complex, the rings do not have upper adjacent cells.

Lower Neighbourhood These are the cells of the same dimension as σ that share a lower dimensional cell on their boundary: $\mathcal{N}^\downarrow(\sigma) = \{\tau \mid \exists \delta : \delta \triangleleft \sigma \wedge \delta \triangleleft \tau\}$. For instance, as shown in the fourth column of Fig. 1, the lower adjacent cells of an edge e_i are the edges that share a common vertex with e_i and the lower adjacent cells of a ring r_i are the rings that have a common edge on their boundary. In any case, the vertices of a regular cell complex do not have a lower neighbourhood.

After defining the structural and neighbourhood elements of a cell complex, we now address how to represent signals over it. A cell signal is defined as a mapping from the set of all the cells contained in the complex to a multi-dimensional feature vector [19].

Definition 3 (Signals Over Cell Complexes). *Let \mathcal{C} be a cell-complex and let \mathcal{P}_C be its indexing set. A cell signal is defined as a map $h_\sigma : \mathcal{P}_C \rightarrow \mathbb{R}^d$ that assigns a d -dimensional feature vector to each cell σ of the complex.*

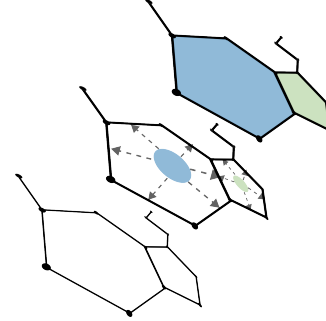


Figure 2: Cellular lifting process. Given an input graph \mathcal{G} , we attach closed two-dimensional rings to the boundary of the induced cycles of \mathcal{G} . The result is a 2D regular cell complex \mathcal{C} .

3 Supramolecular Chemistry

Supramolecular chemistry [20], often referred to as the "*chemistry beyond the molecule*", explores the intricacies of molecules connected through various weak bonds of differing strengths. These spontaneous secondary interactions include hydrogen bonding, dipole-dipole, charge transfer, van der Waals, and $\pi - \pi$ stacking interactions. The presence of numerous $\pi - \pi$ stacking interactions is particularly significant in this context, as the overall system can be seen as a regular cell complex structure. Supramolecular assemblies often exhibit complex chemical architectures and high-order self-assembly, giving rise to molecular machines [21], gas absorption [22], high-tech molecular sensing systems [23], nanoreactors [24], chemical catalysis [25] and drug delivery systems [26]. Intriguingly, molecular shape serves as a design principle, thanks to the self-assembly [27] and self-healing [28] properties of supramolecules.

3.1 Long-Range Interactions

Long-range interactions play a key role in supramolecular chemistry. They can be intended as the dependency of certain molecular properties on elements that are "*far away*" within a chemical system [29]. Of particular interest in this context are the long-range interactions that arise in oxygenic photosynthesis. This is the process by which light energy is converted into chemical energy in the form of glucose or other sugars [30]. This process is mediated by Chlorophyll-a (Fig.3), a cyclic tetrapyrrole molecule. Through its extensive conjugated π -system, Chlorophyll-a represents the basic building block of a photosystem. During photosynthesis, when a photon strikes a molecule of Chlorophyll-a, it excites an electron to a higher energy state. The energy produced is transferred from molecule to molecule within the light-harvesting complex via resonance energy transfer. Throughout the whole process, the energy transfer process is materialised as a quantum-coherent phenomenon [31], that is where long-range interactions become crucial. Being able to capture them could lead to a positive impact in the development of efficient artificial photosynthetic systems [32] and enhance solar energy technologies [33].

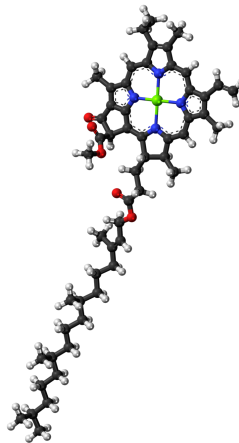


Figure 3: Structure of Chlorophyll-a, the most common molecule in photosynthetic organisms.

On Oversquashing in Molecular Graphs To capture interactions in molecular graphs, in the last years we have seen *Message Passing Neural Networks* (MPNNs) [1] taken as a reference model with remarkable results. These are a class of Graph Neural Networks (GNNs) that update the spatial representation of a node u with layers of the form:

$$\mathbf{h}_u^{l+1} = U\left(\mathbf{h}_u^l, \text{AGG}_{v \in \mathcal{N}(u)}\left(\mathbf{h}_v^l\right)\right), \quad (1)$$

where U is a function that *updates* the node's current features with messages from its neighbours and AGG is a *permutation-invariant aggregation function*. When it is required to aggregate information between nodes located in remote parts of the graph, MPNNs as in Eq. 1 are susceptible to bottlenecks. These bottlenecks are manifested as an exponentially increasing amount of information constrained into vectors with a fixed representation. This is known in the literature as *Oversquashing* [34, 35], a phenomenon that leads to sub-optimal performance when the prediction task is highly reliant on long-range interactions. Oversquashing arises in MPNNs because the propagation of information happens between nodes that are connected through edges, which induces a computational graph directly mirroring the input graph structure.

Message passing schemes on complex topological spaces or *Topological Message Passing* [36, 14, 12] mitigate this issue by not just considering nodes (0-cells) and edges (1-cells), but also involving higher-dimensional elements such as rings (2-cells). With a richer topological structure, the messages can be propagated through these higher-dimensional cells, effectively providing shortcuts or additional routes for information flow. With this construction, the underlying computational graph is no longer coupled with the input graph structure.

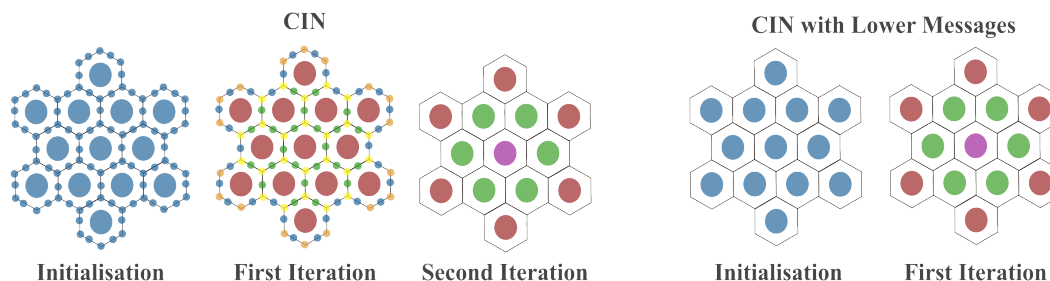


Figure 5: In molecular graphs featuring regions with a high concentration of rings, incorporating lower messages into cellular isomorphism networks expedites the convergence of the 2-cell colours.

3.2 Group Interactions

As long-range interactions, group interactions play a fundamental role in chemical and biological processes. One example is the case of aromatic stacking. Aromatic stacking refers to the non-covalent interactions between aromatic rings, such as those found in the amino acid tryptophan or the nucleotide bases of DNA [37]. These interactions are essential in various biological processes, including protein folding, DNA/RNA structure, and ligand-receptor interactions [38]. Another example is given by the Polycyclic Aromatic Hydrocarbons (PAHs) as they play a significant role in astrophysics and astrobiology. PAHs (Fig. 4) are thought to be among the most abundant and widespread organic molecules in the universe. They are identified in space via their unique infrared emission spectra [39] and can form in the extreme conditions of space. Studying them can potentially contribute to our understanding of the formation of life’s essential building blocks.

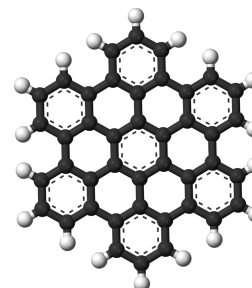


Figure 4: Representation of hexabenzocoronene, a polycyclic aromatic hydrocarbon.

On the convergence speed of Cellular Isomorphism Networks Cellular Isomorphism Networks (CINs) [14] are known to be powerful architectures able to model higher-order signals using a hierarchical message-passing procedure on cell complexes. Analysing the colouring procedure of CINs, the edges must first get the messages coming from the upper neighbourhood and only at the next iteration they can refine the colour of the rings (Fig. 5 (left)). Although this colouring refinement procedure holds the same expressive power ([14], Thm. 7), is it possible to reach a *faster convergence* by including messages coming from the lower neighbourhood of the cells. This allows for a direct interaction between the rings of the complex which removes the bottleneck caused by edges waiting for upper messages before updating ring colours (Fig. 5 (right)).

4 Enhancing Topological Message Passing

In this section, we will describe our enhanced topological message-passing scheme that broadens the exchange of information within the cell complex. In particular, our enhancement consists of the inclusion of lower messages in the scheme proposed in [14]. As we will show later in the section, including lower messages will let the information flow within a broader neighbourhood of the complex, enabling group interaction via the messages exchanged between the rings that are lower adjacent and escaping potential bottlenecks [34] via messages between lower adjacent edges.

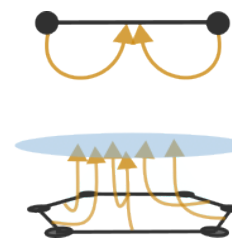


Figure 6: Boundary messages received by an edge (top) and a ring (bottom).

4.1 Boundary Messages

These are the messages that each cell σ receives from its boundary elements $\tau \in \mathcal{B}(\sigma)$. We denote the information coming from the boundary of σ as $m_{\mathcal{B}}(\sigma)$ and consists in a permutation invariant aggregation that takes as

input all the *boundary messages* $M_{\mathcal{B}}$ between the feature vector h_{σ} and all the feature vectors of its boundary elements, h_{τ} as in Fig.6. Formally:

$$m_{\mathcal{B}}^{l+1}(\sigma) = \text{AGG}_{\tau \in \mathcal{B}(\sigma)} \left(M_{\mathcal{B}}(h_{\sigma}^l, h_{\tau}^l) \right).$$

This operation lifts the information from lower cells to higher-order ones, facilitating effective bottom-up communication across the complex. Leveraging the theory developed in [40] for graphs and later on in [14] for regular cell complexes, to maximize the representational power of the underlying network, the function $m_{\mathcal{B}}$ is implemented using a Multi-Layer Perceptron (MLP) with 2 layers.

4.2 Upper Messages

These are the messages that each cell σ receives from its upper neighbouring cells $\tau \in \mathcal{N}^{\uparrow}(\sigma)$ (i.e., the blue arrows in Fig.7) and from common co-boundary cells $\delta \in \mathcal{Co}(\sigma, \tau)$ (i.e., the purple arrows in Fig.7). We denote the information coming from the upper neighbourhood of σ and the common co-boundary elements as $m_{\mathcal{N}^{\uparrow}}$. It consists in a permutation invariant aggregation that takes as input all the *upper messages* $M_{\mathcal{N}^{\uparrow}}$ between the feature vector h_{σ} , all the feature vectors in its upper neighbourhood h_{τ} and all the cells in the common co-boundary neighbourhood, h_{δ} . Formally:

$$m_{\mathcal{N}^{\uparrow}}^{l+1}(\sigma) = \text{AGG}_{\substack{\tau \in \mathcal{N}^{\uparrow}(\sigma) \\ \delta \in \mathcal{Co}(\sigma, \tau)}} \left(M_{\mathcal{N}^{\uparrow}}(h_{\sigma}^l, h_{\tau}^l, h_{\delta}^l) \right).$$

This operation will let the information flow within a *narrow* neighbourhood of σ , ensuring consistency and coherence with respect to the underlying topology of the complex. We implement the function $m_{\mathcal{N}^{\uparrow}}$ using a 2-Layer MLP and $M_{\mathcal{N}^{\uparrow}}$ is represented as a single dense layer followed by a point-wise non-linearity.

4.3 Lower Messages

These are the messages that each cell σ receives from its lower neighbouring cells $\tau \in \mathcal{N}^{\downarrow}(\sigma)$ (i.e., the red arrows in Fig.8) and from common boundary cells $\delta \in \mathcal{B}(\sigma, \tau)$ (i.e., the green arrows in Fig.8). We denote a function that aggregates the information coming from the upper neighbourhood of σ and the common co-boundary elements as $m_{\mathcal{N}^{\downarrow}}$. It consists in a permutation invariant aggregation that takes as input all the *lower messages* $M_{\mathcal{N}^{\downarrow}}$ between the feature vector h_{σ} , all the feature vectors in its lower neighbourhood h_{τ} and all the cells in the common boundary neighbourhood, h_{δ} . Formally:

$$m_{\mathcal{N}^{\downarrow}}^{l+1}(\sigma) = \text{AGG}_{\substack{\tau \in \mathcal{N}^{\downarrow}(\sigma) \\ \delta \in \mathcal{B}(\sigma, \tau)}} \left(M_{\mathcal{N}^{\downarrow}}(h_{\sigma}^l, h_{\tau}^l, h_{\delta}^l) \right).$$

As pictorially shown in Fig.8 (top), this operation would help a *broader* diffusion of the information between edges that are not necessarily part of a ring. Also, it will let the rings of the complex communicate directly (Fig.8 (bottom)). Similarly to the upper messages, we implement $m_{\mathcal{N}^{\downarrow}}$ using a MLP with 2 layers. The function $M_{\mathcal{N}^{\downarrow}}$ is implemented using a single dense layer followed by a point-wise non-linearity.

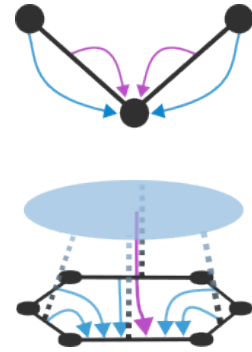


Figure 7: Upper messages are sent to a node (top) and to an edge (bottom). Co-boundary messages are shown in purple.

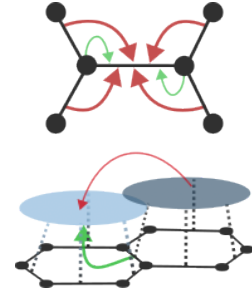


Figure 8: Lower messages are sent to an edge (top) and to a ring (bottom). Boundary messages are shown in green.

4.4 Update and Readout

Update and Readout operations are performed in line with [14]. The exception is that in our case, the update function receives additional information provided by the messages that a cell σ receives from its lower neighbourhood:

$$h_{\sigma}^{l+1} = U\left(h_{\sigma}^l, m_{\mathcal{B}}^l(\sigma), m_{\mathcal{N}^{\uparrow}}^{l+1}(\sigma), m_{\mathcal{N}^{\downarrow}}^{l+1}(\sigma)\right). \quad (2)$$

We represent the update function U using a single fully connected layer followed by a point-wise non-linearity that uses a different set of parameters for each layer of the model and for each dimension of the complex.

After L layers, we compute the representation of the complex \mathcal{C} as:

$$h_{\mathcal{C}} = R\left(\{\{\{h_{\sigma}^L\}\}_{dim(\sigma)=0}\}^2\right), \quad (3)$$

where $\{\{h_{\sigma}^L\}\}$ is the multi-set of cell’s features at layer L . In practice, the representation of the complex is computed in two stages: first, for each dimension of the complex, we compute the representation of the cells at dimension k by applying a mean or sum readout operation. This results in one representation for the vertices $h_{\mathcal{V}}$, one for the edges $h_{\mathcal{E}}$ and one for the rings $h_{\mathcal{R}}$. Then, we compute a representation for the complex \mathcal{C} as: $h_{\mathcal{C}} = \text{MLP}_{R,\mathcal{V}}(h_{\mathcal{V}}) + \text{MLP}_{R,\mathcal{E}}(h_{\mathcal{E}}) + \text{MLP}_{R,\mathcal{R}}(h_{\mathcal{R}})$, where each $\text{MLP}_{R,\cdot}$ is implemented as a single fully-connected layer followed by a non-linearity. Finally, $h_{\mathcal{C}}$ is forwarded to a final dense layer to obtain the predictions.

A neural architecture that updates the cell’s representation using the message passing scheme defined in Eq. 2 and obtains complex-wise representations as in Eq. 3 takes the name of *Enhanced Cell Isomorphism Network* (CIN++). The expressive power of CIN++ can then be directly inferred from the expressivity results reported in [14].

Theorem 1. *Let $\mathcal{F} : \mathcal{C} \rightarrow \mathbb{R}^d$ be a CIN++ network. With a sufficient number of layers and injective neighbourhood aggregators \mathcal{F} is able to map any pair of complexes $(\mathcal{C}_1, \mathcal{C}_2)$ in an embedding space that the Cellular Weisfeiler-Lehman (CWL) test is able to tell if \mathcal{C}_1 and \mathcal{C}_2 are non-isomorphic.*

5 Experiments

In this section, we validate the properties of the proposed message-passing scheme in different real-world scenarios involving graph-structured data. We focus our experiments on a large-scale molecular benchmark (ZINC) [61] and a long-range graph benchmark (Peptides) [62]. Unless otherwise specified, in each Multi-Layer Perceptron, we apply Batch Normalization [63] between the linear transformations and ReLU activations as used Adam [64] with a starting learning rate of 0.001 that is halved whenever the validation loss reaches a plateau after a patience value we set to 20. We used an early stopping criterion that terminates the training when the learning rate reaches a threshold. Unless stated otherwise, we employ $1e^{-5}$ as the early stopping threshold.

5.1 Large-Scale Molecular Benchmarks

We evaluate topological message passing on a large-scale molecular benchmark from the ZINC database [65]. The benchmark is composed of two datasets: *ZINC-Full* (consisting of 250K molecular graphs) and *ZINC-Subset* (an extract of 12k graphs from ZINC-Full) from [61]. In these experiments, we used the same experimental setup of [14] with the exception that we used 3 layers with a hidden dimension of 64. This restricts the parameter budget of our model to have nearly 500K parameters. We follow the training and evaluation procedures in [61]. All results are illustrated in Tab. 1. *Without any use of feature augmentation* such as positional encoding, our model exhibits particularly strong performance on these benchmarks: it attains state-of-the-art results by a significant margin on *ZINC-Subset*, outperforming other models by a significant margin and is on par with the best baselines for *ZINC-Full*.

Table 1: Performance results on ZINC benchmark. We use gold ●, silver ●, and bronze ● colors to indicate the best performance.

Method	Model	Time (s)	Params	Test MAE	
				ZINC-Subset	ZINC-Full
MPNNs	GIN [41]	8.05	509,549	0.526±0.051	0.088±0.002
	GraphSAGE [42]	6.02	505,341	0.398±0.002	0.126±0.003
	GAT [43]	8.28	531,345	0.384±0.007	0.111±0.002
	GCN [44]	5.85	505,079	0.367±0.011	0.113±0.002
	MoNet [45]	7.19	504,013	0.292±0.006	0.090±0.002
	GatedGCN-PE[46]	10.74	505,011	0.214±0.006	-
	MPNN(sum) [1]	-	480,805	0.145±0.007	-
	PNA [47]	-	387,155	0.142±0.010	-
Higher-order GNNs	RingGNN [48]	178.03	527,283	0.353±0.019	-
	3WLGNN [49]	179.35	507,603	0.303±0.068	-
Substructure GNNs	GSN [50]	-	~500k	0.101±0.010	-
Subgraph GNNs	NGNN [51]	-	~500k	0.111±0.003	0.029±0.001
	DSS-GNN [52]	-	445,709	0.097±0.006	-
	GNN-AK [53]	-	~500k	0.105±0.010	-
	GNN-AK+ [53]	-	~500k	0.091±0.011	-
	SUN [54]	15.04	526,489	0.083±0.003	-
Graph Transformers	GT [55]	-	588,929	0.226±0.014	-
	SAN [56]	-	508,577	0.139±0.006	-
	Graphormer [57]	12.26	489,321	0.122±0.006	0.052±0.005
	URPE [58]	12.40	491,737	0.086±0.007	0.028±0.002
GD-WL	Graphormer-GD [59]	12.52	502,793	0.081±0.009	0.025±0.004
Topological NNs	CIN-Small [60]	-	~100k	0.094±0.004	0.044±0.003
	CIN++ (ours)	8.29	501,967	0.077±0.004	0.027±0.007

Table 2: Performance results for Peptides-func (graph classification) and Peptides-struct (graph regression). Best scores are highlighted using gold ●, silver ●, and bronze ● colors.

Model	Peptides-func		Peptides-struct	
	Train AP	Test AP \uparrow	Train MAE	Test MAE \downarrow
MLP	0.4217±0.0049	0.4060±0.0021	0.4273±0.0011	0.4351±0.0008
GCN	0.8840±0.0131	0.5930±0.0023	0.2939±0.0055	0.3496±0.0013
GCNII	0.7271±0.0278	0.5543±0.0078	0.2957±0.0025	0.3471±0.0010
GINE	0.7682±0.0154	0.5498±0.0079	0.3116±0.0047	0.3547±0.0045
GatedGCN	0.8695±0.0402	0.5864±0.0077	0.2761±0.0032	0.3420±0.0013
GatedGCN+RWSE	0.9131±0.0321	0.6069±0.0035	0.2578±0.0116	0.3357±0.0006
Transformer+LapPE	0.8438±0.0263	0.6326±0.0126	0.2403±0.0066	0.2529±0.0016
SAN+LapPE	0.8217±0.0280	0.6384±0.0121	0.2822±0.0108	0.2683±0.0043
SAN+RWSE	0.8612±0.0219	0.6439±0.0075	0.2680±0.0038	0.2545±0.0012
CIN++ (ours)	0.8943±0.0226	0.6569±0.0117	0.229±0.0079	0.2523±0.0013

5.2 Long-Range Graph Benchmarks

To test the effectiveness of enhanced topological message passing for discovering long-range interactions we evaluate our method on a long-range molecular benchmark [62]. The datasets used from the benchmark are derived from 15,535 peptides that compose the SATPdb database [66]. For this benchmark, we evaluate our method against the tasks of peptides structure prediction (Peptides-struct) and peptides function prediction (Peptides-func). For both datasets, we did not employ any feature augmentation such as positional encoding. We ensured that the parameter budget was constrained to 500K. We repeat the training with 4 different seeds and report the mean of the test AP and MAEs at the time of early stopping. For Peptides-struct, we used a cellular lifting map that considers all the induced cycles of dimension up to 8 as rings. We used 3 layers with 64 as a hidden dimension, a batch size of 128 and a sum aggregation to obtain complex-level embeddings. For Peptides-func, we attach 2 cells to all the induced cycles of dimension up to 6. We used 4 layers with an embedding

dimension of 50, and a batch size of 64. A dropout [67] with a probability of 0.15 is inserted. With respect to the other benchmarks, we set the starting learning rate of $4e - 4$, a weight decay of $5e^{-5}$. The final readout is performed with a mean aggregation. As shown in Tab. 2 we achieve very high performance on these tasks even without any use of feature augmentation.

6 Conclusions, Related Works and Future Developments

Broader Impacts This work provides evidence of how the enhanced topological message-passing scheme proposed in this work allows the integration of local and global information within a cell complex in the context of computational chemistry. In particular, our model captures complex dependencies and long-range interactions more effectively. We foresee the proposed work having a broad impact within the field of computational chemistry, as our scheme offers a robust and versatile approach to predict meaningful properties of chemical systems by accurately modelling complex dependencies and capturing long-range and group interactions.

Related Works In light of Topological Deep Learning being an emerging research area that has been introduced quite recently [68], numerous pioneering works appeared in this field. In [13] the authors proposed a Simplicial Weisfeiler-Lehman (SWL) colouring procedure for distinguishing non-isomorphic simplicial complexes and a provably powerful message passing scheme based on SWL, that generalise Graph Isomorphism Networks [40]. This was later refined in [14], where the authors introduced CW Networks (CWNs), a hierarchical message-passing on cell complexes proven to be strictly more powerful than the WL test and not less powerful than the 3-WL test. In [12], the authors provide a general message-passing mechanism over cell complexes however, they do not study the expressive power of the proposed scheme, nor its complexity. Furthermore, they did not experimentally validate its performance. The works in [69, 70] introduced Neural Sheaf Diffusion Models, neural architectures that learn a sheaf structure on graphs to improve learning performance on transductive tasks in heterophilic graphs. Meanwhile, attentional schemes appeared in topological deep learning in the context of simplicial complexes [71, 72], cellular complexes [19], sheaves [73] and combinatorial complexes [74]. For a more detailed examination of the architectures developed in the field of topological deep learning, we refer the reader to the survey of Papillon [75]. Recent works considered also rings within the message passing scheme by means of Junction Trees (JT) [76] and by augmenting node features with information about cycles [77]. However, it is easy to see that these schemes have a different design than the one provided in this work.

Limitations While our work demonstrates that topological message passing effectively models complex dependencies and long-range interactions in chemical systems, we acknowledge that the complexity of the proposed method inherently increases due to the cellular lifting maps and the additional messages sent throughout the complex. We mitigate this computational overhead by mapping all the graphs present in the datasets into cell complexes in a pre-processing stage and storing them for later use. Additionally, the overhead of our message-passing scheme is mitigated by the fact that the operations within the same layer are naturally decoupled. Efficient network implementations make it possible to update the representation of a cell σ in a concurrent execution [78], amortizing the cost to be proportional to the largest neighbourhood of σ .

Conclusions Our study has presented an innovative approach to neural networks operating on graph-structured data. Current state-of-the-art models do not naturally account for a principled way to model group interactions. We addressed this by introducing an enhancement of the Topological Message Passing scheme developed in [14]. The newly proposed Topological Message Passing scheme, named CIN++, enables a direct interaction within high-order structures of the underlying cell complex, by letting messages flow within its lower neighbourhood without sacrificing the model’s expressivity. By allowing the exchange of messages between higher-order structures, we significantly enhance the model’s capacity to capture multi-way relationships in the data. We have demonstrated that the ability to model long-range and group interactions is critical for capturing real-world chemistry-related problems. In particular, the natural affinity of cellular complexes for representing higher-dimensional structures and topological features will provide a more detailed understanding of complex chemical systems compared to traditional models.

References

- [1] James Gilmer, Samuel S. Schoenholz, Patrick F. Riley, Oriol Vinyals, and George E. Dahl. Neural message passing for quantum chemistry. In *International Conference on Machine Learning*, pages 1263–1272. PMLR, 2017.
- [2] Wei Fan, Yiqun Ma, Qing Li, Yuan He, Eric Zhao, Jiliang Tang, and Dawei Yin. Graph neural networks for social recommendation. In *The world wide web conference*, 2019.
- [3] Alvaro Sanchez-Gonzalez, Jonathan Godwin, Tobias Pfaff, Rex Ying, Jure Leskovec, and Peter Battaglia. Learning to simulate complex physics with graph networks. In *International conference on machine learning*, pages 8459–8468. PMLR, 2020.
- [4] Marco Gori, Gabriele Monfardini, and Franco Scarselli. A new model for learning in graph domains. In *IEEE International Joint Conference on Neural Networks*, 2005.
- [5] Franco Scarselli, Marco Gori, Antonio C. Tsoi, Markus Hagenbuchner, and Gabriele Monfardini. The graph neural network model. *IEEE Transactions on Neural Networks*, 2008.
- [6] Peter W. Battaglia, Jessica B. Hamrick, Victor Bapst, Alvaro Sanchez-Gonzalez, Vinicius Zambaldi, Mateusz Malinowski, Andrea Tacchetti, David Raposo, Adam Santoro, Ryan Faulkner, et al. Relational inductive biases, deep learning, and graph networks. *arXiv preprint arXiv:1806.01261*, 2018.
- [7] Thomas N. Kipf and Max Welling. Semi-Supervised Classification with Graph Convolutional Networks. In *International Conference on Learning Representations*, 2017.
- [8] Muhan Zhang and Yixin Chen. Link prediction based on graph neural networks. *Advances in Neural Information Processing Systems*, 2018.
- [9] John Jumper, Richard Evans, Alexander Pritzel, Tim Green, Michael Figurnov, Olaf Ronneberger, Kathryn Tunyasuvunakool, Ruth Bates, Augustin Židek, Artur Potapenko, et al. Highly accurate protein structure prediction with alphafold. *Nature*, 2021.
- [10] Petar Veličković and Charles Blundell. Neural algorithmic reasoning. *Patterns*, 2021.
- [11] Stefania Ebli, Michaël Defferrard, and Gard Spreemann. Simplicial neural networks. In *Advances in Neural Information Processing Systems Workshop on Topological Data Analysis and Beyond*, 2020.
- [12] Mustafa Hajij, Kyle Istvan, and Ghada Zamzmi. Cell complex neural networks. In *Advances in Neural Information Processing Systems Workshop on TDA & Beyond*, 2020.
- [13] Cristian Bodnar, Fabrizio Frasca, Yu Guang Wang, Nina Otter, Guido Montúfar, Pietro Liò, and Michael Bronstein. Weisfeiler and lehman go topological: Message passing simplicial networks. In *International Conference on Machine Learning*, 2021.
- [14] Cristian Bodnar, Fabrizio Frasca, Nina Otter, Yu Guang Wang, Pietro Liò, Guido Montúfar, and Michael Bronstein. Weisfeiler and lehman go cellular: Cw networks. In *Advances in Neural Information Processing Systems*, 2021.
- [15] Chad Giusti, Robert Ghrist, and Danielle S. Bassett. Two’s company, three (or more) is a simplex. *Journal of computational neuroscience*, 2016.
- [16] Renaud Lambiotte, Martin Rosvall, and Ingo Scholtes. From networks to optimal higher-order models of complex systems. *Nature physics*, 2019.
- [17] Richard Sever and Joan S Brugge. Signal transduction in cancer. *Cold Spring Harbor perspectives in medicine*, 2015.
- [18] Jakob Hansen and Robert Ghrist. Toward a spectral theory of cellular sheaves. *Journal of Applied and Computational Topology*, 2019.
- [19] Lorenzo Giusti, Claudio Battiloro, Lucia Testa, Paolo Di Lorenzo, Stefania Sardellitti, and Sergio Barbarossa. Cell attention networks, 2022.

- [20] Jonathan W Steed and Jerry L Atwood. *Supramolecular chemistry*. John Wiley & Sons, 2022.
- [21] Ben L Feringa and Wesley R Browne. *Molecular switches*. John Wiley & Sons, 2011.
- [22] Andrew R Millward and Omar M Yaghi. Metal-organic frameworks with exceptionally high capacity for storage of carbon dioxide at room temperature. *Journal of the American Chemical Society*, 127(51):17998–17999, 2005.
- [23] Mark D Allendorf, Christina A Bauer, RK Bhakta, and RJT Houk. Luminescent metal–organic frameworks. *Chemical Society Reviews*, 38(5):1330–1352, 2009.
- [24] Elio Mattia and Sijbren Otto. Supramolecular systems chemistry. *Nature nanotechnology*, 10(2):111–119, 2015.
- [25] JeongYong Lee, Omar K Farha, John Roberts, Karl A Scheidt, SonBinh T Nguyen, and Joseph T Hupp. Metal–organic framework materials as catalysts. *Chemical Society Reviews*, 38(5):1450–1459, 2009.
- [26] Matthew J Webber and Robert Langer. Drug delivery by supramolecular design. *Chemical Society Reviews*, 46(21):6600–6620, 2017.
- [27] George M Whitesides and Bartosz Grzybowski. Self-assembly at all scales. *Science*, 295(5564):2418–2421, 2002.
- [28] Scott R White, Nancy R Sottos, Philippe H Geubelle, Jeffrey S Moore, Michael R Kessler, SR Sriram, Eric N Brown, and S Viswanathan. Autonomic healing of polymer composites. *Nature*, 409(6822):794–797, 2001.
- [29] Harry B Gray and Jay R Winkler. Long-range electron transfer. *Proceedings of the National Academy of Sciences*, 102(10):3534–3539, 2005.
- [30] James Barber. Photosynthetic energy conversion: natural and artificial. *Chemical Society Reviews*, 38(1):185–196, 2009.
- [31] Gregory S Engel, Tessa R Calhoun, Elizabeth L Read, Tae-Kyu Ahn, Tomáš Mančal, Yuan-Chung Cheng, Robert E Blankenship, and Graham R Fleming. Evidence for wavelike energy transfer through quantum coherence in photosynthetic systems. *Nature*, 446(7137):782–786, 2007.
- [32] Devens Gust, Thomas A Moore, and Ana L Moore. Mimicking photosynthetic solar energy transduction. *Accounts of Chemical Research*, 34(1):40–48, 2001.
- [33] Martin Green, Ewan Dunlop, Jochen Hohl-Ebinger, Masahiro Yoshita, Nikos Kopidakis, and Xiaojing Hao. Solar cell efficiency tables (version 57). *Progress in photovoltaics: research and applications*, 29(1):3–15, 2021.
- [34] Uri Alon and Eran Yahav. On the bottleneck of graph neural networks and its practical implications. *International Conference on Learning Representations*, 2021.
- [35] Francesco Di Giovanni, Lorenzo Giusti, Federico Barbero, Giulia Luise, Pietro Lio, and Michael Bronstein. On over-squashing in message passing neural networks: The impact of width, depth, and topology. In *International Conference on Machine Learning*, 2023.
- [36] Cristian Bodnar, Fabrizio Frasca, Yuguang Wang, Nina Otter, Guido F Montufar, Pietro Lio, and Michael Bronstein. Weisfeiler and leman go topological: Message passing simplicial networks. In *International Conference on Machine Learning*, pages 1026–1037. PMLR, 2021.
- [37] Christopher A Hunter and Jeremy KM Sanders. The nature of. pi.-. pi. interactions. *Journal of the American Chemical Society*, 112(14):5525–5534, 1990.
- [38] Emmanuel A. Meyer, Ronald K. Castellano, and François Diederich. Interactions with aromatic rings in chemical and biological recognition. *Angewandte Chemie International Edition*, 42(11):1210–1250, 2003. doi: <https://doi.org/10.1002/anie.200390319>. URL <https://onlinelibrary.wiley.com/doi/abs/10.1002/anie.200390319>.

- [39] Scott A Sandford, Max P Bernstein, and Christopher K Materese. The infrared spectra of polycyclic aromatic hydrocarbons with excess peripheral h atoms (hn-pahs) and their relation to the 3.4 and 6.9 μm pah emission features. *The Astrophysical Journal Supplement Series*, 205(1):8, 2013.
- [40] Keyulu Xu, Weihua Hu, Jure Leskovec, and Stefanie Jegelka. How powerful are graph neural networks? In *International Conference on Learning Representations*, 2019.
- [41] Keyulu Xu, Weihua Hu, Jure Leskovec, and Stefanie Jegelka. How powerful are graph neural networks? In *International Conference on Learning Representations*, 2019.
- [42] William L. Hamilton, Rex Ying, and Jure Leskovec. Inductive representation learning on large graphs. In *Advances in Neural Information Processing Systems*, volume 30, pages 1025–1035, 2017.
- [43] Petar Veličković, Guillem Cucurull, Arantxa Casanova, Adriana Romero, Pietro Liò, and Yoshua Bengio. Graph attention networks. In *International Conference on Learning Representations*, 2018.
- [44] Thomas N. Kipf and Max Welling. Semi-supervised classification with graph convolutional networks. In *International Conference on Learning Representations*, 2017.
- [45] Federico Monti, Davide Boscaini, Jonathan Masci, Emanuele Rodola, Jan Svoboda, and Michael M Bronstein. Geometric deep learning on graphs and manifolds using mixture model cnns. In *Proceedings of the IEEE conference on computer vision and pattern recognition*, pages 5115–5124, 2017.
- [46] Xavier Bresson and Thomas Laurent. Residual gated graph convnets. *arXiv preprint arXiv:1711.07553*, 2017.
- [47] Gabriele Corso, Luca Cavalleri, Dominique Beaini, Pietro Liò, and Petar Veličković. Principal neighbourhood aggregation for graph nets. *Advances in Neural Information Processing Systems*, 33:13260–13271, 2020.
- [48] Zhengdao Chen, Soledad Villar, Lei Chen, and Joan Bruna. On the equivalence between graph isomorphism testing and function approximation with gnns. *Advances in neural information processing systems*, 32, 2019.
- [49] Haggai Maron, Heli Ben-Hamu, Hadar Serviansky, and Yaron Lipman. Provably powerful graph networks. *Advances in Neural Information Processing Systems*, 32:2156–2167, 2019.
- [50] Giorgos Bouritsas, Fabrizio Frasca, Stefanos Zafeiriou, and Michael Bronstein. Improving graph neural network expressivity via subgraph isomorphism counting. *IEEE Transactions on Pattern Analysis and Machine Intelligence*, 2022.
- [51] Muhan Zhang and Pan Li. Nested graph neural networks. In *Advances in Neural Information Processing Systems*, volume 34, pages 15734–15747, 2021.
- [52] Beatrice Bevilacqua, Fabrizio Frasca, Derek Lim, Balasubramaniam Srinivasan, Chen Cai, Gopinath Balamurugan, Michael M Bronstein, and Haggai Maron. Equivariant subgraph aggregation networks. In *International Conference on Learning Representations*, 2022.
- [53] Lingxiao Zhao, Wei Jin, Leman Akoglu, and Neil Shah. From stars to subgraphs: Uplifting any gnn with local structure awareness. In *International Conference on Learning Representations*, 2022.
- [54] Fabrizio Frasca, Beatrice Bevilacqua, Michael Bronstein, and Haggai Maron. Understanding and extending subgraph gnns by rethinking their symmetries. *arXiv preprint arXiv:2206.11140*, 2022.
- [55] Vijay Prakash Dwivedi and Xavier Bresson. A generalization of transformer networks to graphs. *AAAI Workshop on Deep Learning on Graphs: Methods and Applications*, 2021.

- [56] Devin Kreuzer, Dominique Beaini, Will Hamilton, Vincent Létourneau, and Prudencio Tossou. Rethinking graph transformers with spectral attention. In *Advances in Neural Information Processing Systems*, volume 34, 2021.
- [57] Chengxuan Ying, Tianle Cai, Shengjie Luo, Shuxin Zheng, Guolin Ke, Di He, Yanming Shen, and Tie-Yan Liu. Do transformers really perform badly for graph representation? *Advances in Neural Information Processing Systems*, 34, 2021.
- [58] Shengjie Luo, Shanda Li, Shuxin Zheng, Tie-Yan Liu, Liwei Wang, and Di He. Your transformer may not be as powerful as you expect. *arXiv preprint arXiv:2205.13401*, 2022.
- [59] Bohang Zhang, Shengjie Luo, Liwei Wang, and Di He. Rethinking the expressive power of gnns via graph biconnectivity, 2023.
- [60] Cristian Bodnar, Fabrizio Frasca, Nina Otter, Yu Guang Wang, Pietro Liò, Guido Montufar, and Michael M. Bronstein. Weisfeiler and leman go cellular: CW networks. In *Advances in Neural Information Processing Systems*, volume 34, 2021.
- [61] Vijay Prakash Dwivedi, Chaitanya K Joshi, Thomas Laurent, Yoshua Bengio, and Xavier Bresson. Benchmarking graph neural networks. *arXiv preprint arXiv:2003.00982*, 2020.
- [62] Vijay Prakash Dwivedi, Ladislav Rampásek, Michael Galkin, Ali Parviz, Guy Wolf, Anh Tuan Luu, and Dominique Beaini. Long range graph benchmark. *Advances in Neural Information Processing Systems*, 35:22326–22340, 2022.
- [63] Sergey Ioffe and Christian Szegedy. Batch normalization: Accelerating deep network training by reducing internal covariate shift. In *International Conference on Machine Learning*, 2015.
- [64] Diederik P Kingma and Jimmy Ba. Adam: A method for stochastic optimization. In *International Conference on Learning Representations*, 2015.
- [65] Teague Sterling and John J. Irwin. ZINC 15 – ligand discovery for everyone. *Journal of Chemical Information and Modeling*, 55(11):2324–2337, 11 2015. doi: 10.1021/acs.jcim.5b00559. URL <https://doi.org/10.1021/acs.jcim.5b00559>.
- [66] Sandeep Singh, Kumardeep Chaudhary, Sandeep Kumar Dhanda, Sherry Bhalla, Salman Sadullah Usmani, Ankur Gautam, Abhishek Tuknait, Piyush Agrawal, Deepika Mathur, and Gajendra PS Raghava. SATPdb: a database of structurally annotated therapeutic peptides. *Nucleic acids research*, 44(D1):D1119–D1126, 2016.
- [67] Nitish Srivastava, Geoffrey Hinton, Alex Krizhevsky, Ilya Sutskever, and Ruslan Salakhutdinov. Dropout: a simple way to prevent neural networks from overfitting. *The journal of machine learning research*, 15(1):1929–1958, 2014.
- [68] Mustafa Hajij, Ghada Zamzmi, Theodore Papamarkou, Nina Miolane, Aldo Guzmán-Sáenz, Karthikeyan Natesan Ramamurthy, Tolga Birdal, Tamal K Dey, Soham Mukherjee, Shreyas N Samaga, et al. Topological deep learning: Going beyond graph data.
- [69] Cristian Bodnar, Francesco Di Giovanni, Benjamin Paul Chamberlain, Pietro Lio, and Michael M. Bronstein. Neural sheaf diffusion: A topological perspective on heterophily and oversmoothing in GNNs. In *Advances in Neural Information Processing Systems*, 2022.
- [70] Julian Suk, Lorenzo Giusti, Tamir Hemo, Miguel Lopez, Konstantinos Barmpas, and Cristian Bodnar. Surfing on the neural sheaf. In *Advances in Neural Information Processing Systems Workshop on Symmetry and Geometry in Neural Representations*, 2022.
- [71] Lorenzo Giusti, Claudio Battiloro, Paolo Di Lorenzo, Stefania Sardellitti, and Sergio Barbarossa. Simplicial attention neural networks, 2022.
- [72] Christopher Wei Jin Goh, Cristian Bodnar, and Pietro Liò. Simplicial attention networks. In *International Conference on Learning Representations Workshop on Geometrical and Topological Representation Learning*, 2022.

- [73] Federico Barbero, Cristian Bodnar, Haitz Sáez de Ocáriz Borde, and Pietro Lio. Sheaf attention networks. In *NeurIPS 2022 Workshop on Symmetry and Geometry in Neural Representations*, 2022.
- [74] Mustafa Hajj, Ghada Zamzmiand, Theodore Papamarkou, Nina Miolane, Aldo Guzmán-Sàenz, and Karthikeyan Natesan Ramamurthy. Higher-order attention networks, 2022.
- [75] Mathilde Papillon, Sophia Sanborn, Mustafa Hajj, and Nina Miolane. Architectures of topological deep learning: A survey on topological neural networks. *arXiv preprint arXiv:2304.10031*, 2023.
- [76] Matthias Fey, Jan-Gin Yuen, and Frank Weichert. Hierarchical inter-message passing for learning on molecular graphs. In *International Conference on Machine Learning Graph Representation Learning and Beyond (GRL+) Workshop*, 2020.
- [77] Giorgos Bouritsas, Fabrizio Frasca, Stefanos Zafeiriou, and Michael M Bronstein. Improving graph neural network expressivity via subgraph isomorphism counting. *arXiv:2006.09252*, 2020.
- [78] Maciej Besta and Torsten Hoefler. Parallel and distributed graph neural networks: An in-depth concurrency analysis, 2022.
- [79] Christopher Morris, Martin Ritzert, Matthias Fey, William L Hamilton, Jan Eric Lenssen, Gaurav Rattan, and Martin Grohe. Weisfeiler and Leman go neural: Higher-order graph neural networks. In *AAAI*, volume 33, pages 4602–4609, 2019.
- [80] Adam Paszke, Sam Gross, Francisco Massa, Adam Lerer, James Bradbury, Gregory Chanan, Trevor Killeen, Zeming Lin, Natalia Gimelshein, Luca Antiga, Alban Desmaison, Andreas Kopf, Edward Yang, Zachary DeVito, Martin Raison, Alykhan Tejani, Sasank Chilamkurthy, Benoit Steiner, Lu Fang, Junjie Bai, and Soumith Chintala. PyTorch: An imperative style, high-performance deep learning library. In *Advances in Neural Information Processing Systems*, pages 8024–8035, 2019.
- [81] Matthias Fey and Jan Eric Lenssen. Fast graph representation learning with PyTorch Geometric. In *International Conference on Learning Representations Workshop on Representation Learning on Graphs and Manifolds*, 2019.
- [82] Thomas N Kipf and Max Welling. Semi-supervised classification with graph convolutional networks. In *International Conference on Learning Representations*, 2017.
- [83] Petar Veličković, Guillem Cucurull, Arantxa Casanova, Adriana Romero, Pietro Liò, and Yoshua Bengio. Graph attention networks. In *International Conference on Learning Representations*, 2018.
- [84] Keyulu Xu, Weihua Hu, Jure Leskovec, and Stefanie Jegelka. How powerful are graph neural networks? In *International Conference on Learning Representations*, 2019.
- [85] Gabriele Corso, Luca Cavalleri, Dominique Beaini, Pietro Liò, and Petar Veličković. Principal neighbourhood aggregation for graph nets. In *Advances in Neural Information Processing Systems*, volume 33, pages 13260–13271, 2020.
- [86] Dominique Beaini, Saro Passaro, Vincent Létourneau, William L Hamilton, Gabriele Corso, and Pietro Liò. Directional graph networks. *International Conference on Machine Learning*, 2021.
- [87] Rafael Gómez-Bombarelli, Jennifer N Wei, David Duvenaud, José Miguel Hernández-Lobato, Benjamín Sánchez-Lengeling, Dennis Sheberla, Jorge Aguilera-Iparraguirre, Timothy D Hirzel, Ryan P Adams, and Alán Aspuru-Guzik. Automatic chemical design using a data-driven continuous representation of molecules. *ACS Central Science*, 4(2):268–276, 2018.
- [88] Weihua Hu, Matthias Fey, Marinka Zitnik, Yuxiao Dong, Hongyu Ren, Bowen Liu, Michele Catasta, and Jure Leskovec. Open graph benchmark: Datasets for machine learning on graphs. In *Advances in Neural Information Processing Systems*, 2020.

- [89] Thomas Gärtner, Peter A. Flach, and Stefan Wrobel. On graph kernels: Hardness results and efficient alternatives. In *Learning theory and kernel machines*, pages 129–143. Springer, 2003.
- [90] Nino Shervashidze, SVN Vishwanathan, Tobias Petri, Kurt Mehlhorn, and Karsten Borgwardt. Efficient graphlet kernels for large graph comparison. In *Artificial Intelligence and Statistics*, pages 488–495, 2009.
- [91] Marion Neumann, Roman Garnett, Christian Bauckhage, and Kristian Kersting. Propagation kernels: efficient graph kernels from propagated information. *Machine Learning*, 102(2): 209–245, 2016.
- [92] Nino Shervashidze, Pascal Schweitzer, Erik Jan van Leeuwen, Kurt Mehlhorn, and Karsten M. Borgwardt. Weisfeiler-lehman graph kernels. *Journal of Machine Learning Research*, 12(Sep): 2539–2561, 2011.
- [93] James Atwood and Don Towsley. Diffusion-convolutional neural networks. In *Advances in Neural Information Processing Systems*, pages 1993–2001, 2016.
- [94] Muhan Zhang, Zhicheng Cui, Marion Neumann, and Yixin Chen. An end-to-end deep learning architecture for graph classification. In *AAAI Conference on Artificial Intelligence*, 2018.
- [95] Haggai Maron, Heli Ben-Hamu, Nadav Shamir, and Yaron Lipman. Invariant and equivariant graph networks. In *International Conference on Learning Representations*, 2019.
- [96] Pim de Haan, Taco S. Cohen, and Max Welling. Natural graph networks. *Advances in Neural Information Processing Systems*, 33:3636–3646, 2020.
- [97] Christopher Morris, Nils M Kriege, Franka Bause, Kristian Kersting, Petra Mutzel, and Marion Neumann. Tudataset: A collection of benchmark datasets for learning with graphs. *arXiv preprint arXiv:2007.08663*, 2020.
- [98] Asim Kumar Debnath, Rosa L Lopez de Compadre, Gargi Debnath, Alan J Shusterman, and Corwin Hansch. Structure-activity relationship of mutagenic aromatic and heteroaromatic nitro compounds. correlation with molecular orbital energies and hydrophobicity. *J Med Chem*, 34:786–797, 1991.
- [99] Toivonen Hannu, Ashwin Srinivasan, Ross D. King, Stefan Kramer, and Christoph Helma. Statistical evaluation of the predictive toxicology challenge 2000–2001. *Bioinformatics*, 19: 1183–1193, 2003.
- [100] Nikil Wale, Ian A. Watson, and George Karypis. Comparison of descriptor spaces for chemical compound retrieval and classification. *Knowledge and Information Systems*, 14(3):347–375, 2008.
- [101] Karsten M. Borgwardt, Cheng Soon Ong, Stefan Schönauer, S. V. N. Vishwanathan, Alex J. Smola, and Hans-Peter Kriegel. Protein function prediction via graph kernels. *Bioinformatics*, 21(suppl_1):i47–i56, 2005.

A Glossary

Table 3: Summary of Notations. The first section, *Structural Elements*, details the notation for fundamental mathematical and topological constructs such as graphs, regular cell complexes, and their associated components. The second section, *Functional Elements*, delineates the notation for functional aspects, including feature vectors, information exchange, and various functional operations.

Structural Elements	
$\mathcal{G} = (\mathcal{V}, \mathcal{E})$	A graph, \mathcal{V} and \mathcal{E} are respectively the sets of vertices and edges.
$\mathcal{C} = (\mathcal{V}, \mathcal{E}, \mathcal{R})$	A regular cell complex, \mathcal{R} is the set of rings.
v_i	An element of \mathcal{V} .
$e_i = (v_i, v_j)$	An element of \mathcal{E} .
$r_i = (e_{i_1}, \dots, e_{i_{ r_i }})$	An element of \mathcal{R} . $ r_i $ is the size of the i -th ring.
$\mathcal{B}(\sigma)$	Boundary of σ .
$\mathcal{C}o(\sigma)$	Co-boundary of σ .
$\mathcal{N}^\uparrow(\sigma)$	Upper neighbourhood of σ .
$\mathcal{N}^\downarrow(\sigma)$	Lower neighbourhood of σ .
$\sigma \triangleleft \tau$	Boundary relationship (i.e. $\sigma \in \mathcal{B}(\tau)$).
$\mathcal{B}(\sigma, \tau)$	Boundary elements in common between σ and τ .
$\mathcal{C}o(\sigma, \tau)$	Co-boundary elements in common between σ and τ .
Functional Elements	
h_σ^l	Feature vector of the cell σ at layer l .
$m_{\mathcal{B}}^l(\sigma)$	Information that σ receives from cells $\tau \in \mathcal{B}(\sigma)$ at layer l .
$m_{\mathcal{N}^\uparrow}^l(\sigma)$	Information that σ receives from cells $\tau \in \mathcal{N}^\uparrow(\sigma), \delta \in \mathcal{C}o(\sigma, \tau)$ at layer l .
$m_{\mathcal{N}^\downarrow}^l(\sigma)$	Information that σ receives from cells $\tau \in \mathcal{N}^\downarrow(\sigma), \delta \in \mathcal{B}(\sigma, \tau)$ at layer l .
$M_{\mathcal{B}}$	Boundary message function between σ and $\tau \in \mathcal{B}(\sigma)$.
$M_{\mathcal{N}^\uparrow}$	Upper message function between $\sigma, \tau \in \mathcal{N}^\uparrow(\sigma)$ and $\delta \in \mathcal{C}o(\sigma, \tau)$.
$M_{\mathcal{N}^\downarrow}$	Lower message function between $\sigma, \tau \in \mathcal{N}^\downarrow(\sigma)$ and $\delta \in \mathcal{B}(\sigma, \tau)$.
AGG	Permutation equivariant aggregation function.
U	Update function.
R	Readout function.

B Expressive Power

In this section we analyse the expressive power of enhanced topological message passing. Two complexes \mathcal{C}_1 and \mathcal{C}_2 are said to be *isomorphic* (written $\mathcal{C}_1 \simeq \mathcal{C}_2$) if there exists a bijection $\varphi : \mathcal{P}_{\mathcal{C}_1} \rightarrow \mathcal{P}_{\mathcal{C}_2}$ such that $\sigma \in \mathcal{C}_1 \iff \varphi(\sigma) \in \mathcal{C}_2$ [36, 14]. Also, we say that a cell coloring c *refines* a cell coloring d , written $c \sqsubseteq d$, if $c(\sigma) = c(\tau) \implies d(\sigma) = d(\tau)$ for every $\sigma, \tau \in \mathcal{C}$. Two colorings are *equivalent* if $c \sqsubseteq d$ and $d \sqsubseteq c$, and we write $c \equiv d$ [79].

Proof of Theorem 1. Let c^l be the colouring of CWL [14] at iteration l and h^l the colouring (i.e., the multi-set of features) provided by a CIN++ network at layer l as in Section 4.

To show that CIN++ inherits all the properties of Cellular Isomorphism Networks [14] we must show that our scheme produces a colouring of the complex that satisfies Lemma 26 of [14].

To show $c^t \sqsubseteq h^t$ by induction, let us assume $h^l = h^L$ for all $l > L$, where L is the number of the network's layers. Let also σ, τ be two arbitrary cells with $c_\sigma^{l+1} = c_\tau^{l+1}$. Then, $c_\sigma^l = c_\tau^l$, $c_{\mathcal{B}}^l(\sigma) = c_{\mathcal{B}}^l(\tau)$, $c_{\uparrow}^l(\sigma) = c_{\uparrow}^l(\tau)$ and $c_{\downarrow}^l(\sigma) = c_{\downarrow}^l(\tau)$. By the induction hypothesis, $h_\sigma^l = h_\tau^l$, $h_{\mathcal{B}}^l(\sigma) = h_{\mathcal{B}}^l(\tau)$, $h_{\uparrow}^l(\sigma) = h_{\uparrow}^l(\tau)$ and $h_{\downarrow}^l(\sigma) = h_{\downarrow}^l(\tau)$.

If $l + 1 > L$, then $h_\sigma^{l+1} = h_\sigma^l = h_\tau^l = h_\tau^{l+1}$. Otherwise, h^{l+1} is given by the update function in Equation 2. Given that the inputs passed to these functions are equal for σ and τ , $h_\sigma^{l+1} = h_\tau^{l+1}$.

For showing $h^l \sqsubseteq c^l$, let us suppose the aggregation from Equation 2 is injective and the model is equipped with a sufficient number of layers such that the convergence of the colouring is guaranteed. Let σ, τ be two cells with $h_\sigma^{l+1} = h_\tau^{l+1}$. Then, since the local aggregation is injective $h_\sigma^l = h_\tau^l$, $h_{\mathcal{B}}^l(\sigma) = h_{\mathcal{B}}^l(\tau)$, $h_{\uparrow}^l(\sigma) = h_{\uparrow}^l(\tau)$ and $h_{\downarrow}^l(\sigma) = h_{\downarrow}^l(\tau)$. By the induction hypothesis, $c_\sigma^l = c_\tau^l$, $c_{\mathcal{B}}^l(\sigma) = c_{\mathcal{B}}^l(\tau)$, $c_{\uparrow}^l(\sigma) = c_{\uparrow}^l(\tau)$ and $c_{\downarrow}^l(\sigma) = c_{\downarrow}^l(\tau)$ which implies that $c_\sigma^{l+1} = c_\tau^{l+1}$.

Given that we have shown $c^t \sqsubseteq h^t$ and $h^l \sqsubseteq c^l$, we can conclude that $h^l \equiv c^l$. \square

As a result, we have that CIN++ inherits all the properties of Cellular Isomorphism Networks, in accordance with Lemma 26 from [14].

C Complexity Analysis

In this section we will characterise the complexity of a CIN++ layer in terms of number of messages and number of parameters involved for a two-dimensional regular cell complex \mathcal{C} whose number of cells is denoted with $|\mathcal{C}|$. Let us assume $\sigma \in \mathcal{C}$ be an arbitrary cell of \mathcal{C} such that $\dim(\sigma)$ is either 0, 1 or 2 and $|\mathcal{B}(\sigma)| \leq c_1$ and $|\mathcal{Co}(\sigma)| \leq c_2$, for some constants c_1 and c_2 . Let also $h_\sigma^l \in \mathbb{R}^d$ be the features of the cell σ at layer l .

Boundary Messages The boundary message function is implemented as:

$$m_{\mathcal{B}}^l(\sigma) := \text{MLP}_{\mathcal{B}}^l \left((1 + \epsilon_{\mathcal{B}}) h_\sigma^l + \sum_{\tau \in \mathcal{B}(\sigma)} h_\tau^l \right),$$

where $\text{MLP}_{\mathcal{B}}^l$ has 2 fully-connected layers. Considering that 0-cells (vertices) do not have boundary elements, 1-cells (edges) have only two boundary elements and the maximum ring size of \mathcal{C} is bounded by a small constant [14], we have that the number of boundary messages scales with $\mathcal{O}(|\mathcal{C}|)$. The number of parameter involved in this operation is $\mathcal{O}(d^2)$, provided by the outer Multi-Layer Perceptron (MLP). In this work, we did not employ any parameter sharing across the dimensions of the complex (i.e., we used a distinct perceptron for each layer of the network and for each dimension of the complex).

Upper Messages We implement the upper message function as:

$$m_{\mathcal{N}\uparrow}^l(\sigma) := \text{MLP}_{\mathcal{N}\uparrow}^l \left((1 + \epsilon_{\mathcal{N}\uparrow}) h_\sigma^l + \sum_{\substack{\tau \in \mathcal{N}\uparrow(\sigma) \\ \delta \in \mathcal{Co}(\sigma, \tau)}} \text{MLP}_{M\uparrow}^l(h_\tau^l \parallel h_\delta^l) \right),$$

In this context, $\text{MLP}_{M\uparrow}^l$ denotes a single-layer fully-connected network, complemented by a point-wise non-linearity, while $\text{MLP}_{\mathcal{N}\uparrow}^l$ represents a two-layer Multilayer Perceptron (MLP). As indicated in [14], the amount of upper messages that a cell $\tau \in \mathcal{B}(\sigma)$ exchanges with its adjacent cells is given by $2 \cdot \binom{|\mathcal{B}(\sigma)|}{2}$. Considering the assumption that the boundary of the cells is bounded by a fixed constant, the total number of messages correlates linearly with the magnitude of the complex, that is, the number of cells in \mathcal{C} . The amount of learnable parameters is also on the order of $\mathcal{O}(d^2)$, a consequence of the two MLPs utilized in the message function.

Lower Messages The implementation of the lower message function is as follows:

$$m_{\mathcal{N}\downarrow}^l(\sigma) := \text{MLP}_{\mathcal{N}\downarrow}^l \left((1 + \epsilon_{\mathcal{N}\downarrow}) h_\sigma^l + \sum_{\substack{\tau \in \mathcal{N}\downarrow(\sigma) \\ \delta \in \mathcal{B}(\sigma, \tau)}} \text{MLP}_{M\downarrow}^l(h_\tau^l \parallel h_\delta^l) \right).$$

As for the upper messages, $\text{MLP}_{M\downarrow}^l$ denotes a single-layer fully-connected network, succeeded by a point-wise non-linearity, while $\text{MLP}_{N\downarrow}^l$ represents a two-layer Multilayer Perceptron (MLP). The amount of lower messages that a cell $\tau \in \mathcal{C}o(\sigma)$ exchanges with its neighbours is given by $2 \cdot \binom{|\mathcal{C}o(\sigma)|}{2}$. Since we assumed also that the cells have a number of co-boundary neighbours that is bounded by a fixed constant, the total number of messages scales linearly with the number of cells in the complex. The two MLPs involved in the message function induces an amount of learnable parameters on the order of $\mathcal{O}(d^2)$.

D A Categorical Interpretation: Sheaves

Our method can be seen as a particular case of a message passing scheme over a cellular sheaf. Let \mathcal{C} be a regular cell complex. A cellular sheaf is a mathematical object that attaches data spaces to the cells of \mathcal{C} together with relations that specify when assignments to these data spaces are consistent.

Definition 4 (Cellular Sheaf). [18] A cellular sheaf of vector spaces on a regular cell complex \mathcal{C} is an assignment of a vector space $\mathcal{F}(\sigma)$ to each cell σ of \mathcal{C} together with a linear transformation $\mathcal{F}_{\sigma \triangleleft \tau} : \mathcal{F}(\sigma) \rightarrow \mathcal{F}(\tau)$ for each incident cell pair $\sigma \triangleleft \tau$. These must satisfy both an identity relation $\mathcal{F}_{\sigma \triangleleft \sigma} = \text{id}$ and the composition condition:

$$\rho \triangleleft \sigma \triangleleft \tau \Rightarrow \mathcal{F}_{\rho \triangleleft \tau} = \mathcal{F}_{\sigma \triangleleft \tau} \circ \mathcal{F}_{\rho \triangleleft \sigma}.$$

It is also natural to consider a dual construction to a cellular sheaf to preserve stalk data but reverses the direction of the face poset, and with it, the restriction maps.

Definition 5 (Cellular Cosheaf). [18] A cellular cosheaf of vector spaces on a regular cell complex \mathcal{C} is an assignment of a vector space $\mathcal{F}(\sigma)$ to each cell σ of \mathcal{C} together with linear maps $\mathcal{F}_{\sigma \triangleleft \tau}^{\text{op}} : \mathcal{F}(\tau) \rightarrow \mathcal{F}(\sigma)$ for each incident cell pair $\sigma \triangleleft \tau$ which satisfies the identity ($\mathcal{F}_{\sigma \triangleleft \sigma}^{\text{op}} = \text{id}$) and composition condition:

$$\rho \triangleleft \sigma \triangleleft \tau \Rightarrow \mathcal{F}_{\rho \triangleleft \tau}^{\text{op}} = \mathcal{F}_{\rho \triangleleft \sigma}^{\text{op}} \circ \mathcal{F}_{\sigma \triangleleft \tau}^{\text{op}}.$$

The vector space $\mathcal{F}(\sigma)$ is called the *stalk* of \mathcal{F} at σ and will encode the features supported over σ . The maps $\mathcal{F}_{\sigma \triangleleft \tau}$ and $\mathcal{F}_{\sigma \triangleleft \tau}^{\text{op}}$ are called the *restriction maps* and will provide a principled way to respectively move features from lower dimensional cells to higher dimensional ones and vice-versa.

From a categorical perspective, a cellular sheaf is a functor $\mathcal{F} : \mathcal{P}_{\mathcal{C}} \rightarrow \mathbf{Vect}_{\mathbb{R}}$ that maps the indexing set $\mathcal{P}_{\mathcal{C}}$ to the category of vector spaces over \mathbb{R} while a cellular cosheaf is a functor $\mathcal{F}^{\text{op}} : \mathcal{P}_{\mathcal{C}}^{\text{op}} \rightarrow \mathbf{Vect}_{\mathbb{R}}$ such that, if we consider a two dimensional regular cell complex \mathcal{C} , a sheaf $(\mathcal{F}, \mathbb{R})$ and its dual cosheaf $(\mathcal{F}^{\text{op}}, \mathbb{R})$ on \mathcal{C} , the following diagram commutes:

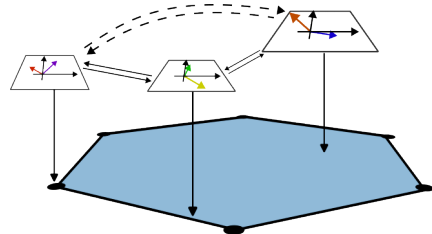
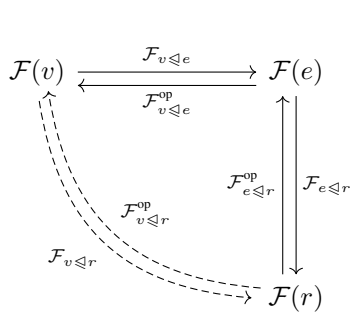


Figure 9: Pictorial example of a sheaf and cosheaf of vector spaces structure on a ring of a regular cell complex \mathcal{C} .

In the given commutative diagram, the arrow is dashed to indicate that the morphism (map) it represents is not explicitly defined in the diagram, but rather it is implied by the other morphisms. In this case, the dashed arrow is used to show the existence of a unique morphism that makes the diagram commute. This relationship is important in the context of cellular sheaves, where these morphisms represent restrictions on different cells and their overlaps. The dashed arrows shows that there's a unique way to go from $\mathcal{F}(v)$ to $\mathcal{F}(r)$ and back that is consistent with the other restrictions, even if it's not directly defined in the diagram.

Table 4: ZINC-Subset (MAE), ZINC-Full (MAE) and Mol-HIV.

Model	ZINC-Subset (MAE ↓)	ZINC-Full (MAE ↓)	MOLHIV (ROC-AUC ↑)
GCN [82]	0.469±0.002	N/A	76.06±0.97
GAT [83]	0.463±0.002	N/A	N/A
GatedGCN [46]	0.363±0.009	N/A	N/A
GIN [84]	0.252±0.014	0.088±0.002	77.07±1.49
PNA [85]	0.188±0.004	N/A	79.05±1.32
DGN [86]	0.168±0.003	N/A	79.70±0.97
HIMP [76]	0.151±0.006	0.036±0.002	78.80±0.82
GSN [77]	0.108±0.018	N/A	77.99±1.00
CIN-small [14]	0.094±0.004	0.044±0.003	80.55±1.04
CIN [14]	0.079±0.006	0.022±0.002	80.94±0.57
CIN++-small (ours)	0.091±0.003	0.044±0.004	80.26±1.02
CIN++ (ours)	0.074±0.004	0.021±0.001	80.63±0.94

E Additional Experimental Details

E.1 Computational Resources and Code Assets

In all experiments we used NVIDIA[®] Tesla V100 GPUs with 5,120 CUDA cores and 32GB GPU memory on a personal computing platform with an Intel[®] Xeon[®] Gold 5218 CPU @ 2.30GHz CPU using Ubuntu 18.04.6 LTS.

The model has been implemented in PyTorch [80] by building on top of CW Networks library³ [14] and PyTorch Geometric library⁴ [81]. High-performance lifting operations use the graph-tool⁵ Python library and are parallelised via Joblib⁶. PyTorch, NumPy, SciPy and Joblib are made available under the BSD license, Matplotlib under the PSF license, graph-tool under the GNU LGPL v3 license. CW Networks and PyTorch Geometric are made available under the MIT license.

E.2 Large Scale Molecular Benchmarks

ZINC The number of nodes (or atoms) in the graphs ranges from 3 to 132, with an average size of approximately 24 nodes. The majority of the graphs have between 10 and 30 nodes. The average degree in the graphs is approximately 2 and the average diameter of the graphs is approximately 12.4 nodes (or atoms) and the maximum diameter was 62 nodes. Regarding the edges (or bonds), the average number of edges in the graphs is approximately 50 composed of 98% by single bonds, while the remaining 2% are aromatic bonds. These are two graph regression task datasets for drug-constrained solubility prediction which have been built on top of the ZINC database provided by the Irwin and Shoichet Laboratories in the Department of Pharmaceutical Chemistry at the University of California, San Francisco (UCSF) [65]. Each graph represents a molecule, where the features over the nodes specify which atom it represents while edge features specify the type of chemical bond between two atoms. Graph-level targets correspond to the penalised water-octanol partition coefficient – logP, an important metric in drug design that depends on chemical structures and molecular properties and characterizes the drug-likeness of a molecule [87].

MOLHIV In our study, we further validate our model using the ogbg-molhiv molecular dataset from the Open Graph Benchmark [88]. Each graph is a representation of a molecule, where the nodes stand for atoms and the edges symbolize chemical bonds. The node features, which are 9-dimensional, include the atomic number, chirality, and other atom-specific attributes such as formal

³<https://github.com/twitter-research/cwn/>

⁴https://github.com/pyg-team/pytorch_geometric/

⁵<https://graph-tool.skewed.de/>

⁶<https://joblib.readthedocs.io/en/latest/>

Table 5: TUDatasets. The first part shows the performance of graph kernel methods. The second assess graph neural networks while the third part is for topological neural networks. We mark the models with highest performance using gold 🏆, silver 🥈, and bronze 🥉 colors.

Model	MUTAG	PTC_MR	PROTEINS	NCI1	NCI109
RWK [89]	79.2±2.1	55.9±0.3	59.6±0.1	>3 days	N/A
GK ($k = 3$) [90]	81.4±1.7	55.7±0.5	71.4±0.3	62.5±0.3	62.4±0.3
PK [91]	76.0±2.7	59.5±2.4	73.7±0.7	82.5±0.5	N/A
WL kernel [92]	90.4±5.7	59.9±4.3	75.0±3.1	86.0±1.8	N/A
DCNN [93]	N/A	N/A	61.3±1.6	56.6±1.0	N/A
DGCNN [94]	85.8±1.8	58.6±2.5	75.5±0.9	74.4±0.5	N/A
IGN [95]	83.9±13.0	58.5±6.9	76.6±5.5	74.3±2.7	72.8±1.5
GIN [84]	89.4±5.6	64.6±7.0	76.2±2.8	82.7±1.7	N/A
PPGNs [49]	90.6±8.7	66.2±6.6	77.2±4.7	83.2±1.1	82.2±1.4
Natural GN [96]	89.4±1.6	66.8±1.7	71.7±1.0	82.4±1.3	N/A
GSN [77]	92.2 ± 7.5	68.2 ± 7.2	76.6 ± 5.0	83.5 ± 2.0	N/A
SIN [13]	N/A	N/A	76.4 ± 3.3	82.7 ± 2.1	N/A
CIN [14]	92.7 ± 6.1	68.2 ± 5.6	77.0 ± 4.3	83.6 ± 1.4	84.0 ± 1.6
CAN [19]	94.1 ± 4.8	72.8 ± 8.3	78.2 ± 2.0	84.5 ± 1.6	83.6 ± 1.2
CIN++ (Ours)	94.4 ± 3.7	73.2 ± 6.4	80.5 ± 3.9	85.3 ± 1.2	84.5 ± 2.4

charge and ring inclusion. The edge features, which are 3-dimensional, incorporate the bond type, bond stereochemistry, and an additional feature that indicates the presence of a conjugated bond. The statistics of the graphs in the dataset are similar to the ones discussed for the ZINC benchmark. The objective is to ascertain the ability of compounds to inhibit HIV replication. We consider a maximum ring size of 6 nodes as 2-cells. Our model’s architecture and hyperparameter settings mirror those referenced in previous studies [14, 76]. In Tab. 4, we present the average test ROC-AUC metrics at the epoch of optimal validation performance across 10 random weight initializations. For this dataset, we experience lower performance than

E.3 Long-Range Molecular Benchmarks

In both tasks of this benchmark, each graph corresponds to a peptide molecule [62]. Peptides, in the realm of biology, are depicted as compact polymers of amino acids, which are covalently bonded through peptide linkages formed between the carboxyl group of one amino acid and the amino group of another. These molecules execute a diverse spectrum of functions in living organisms, serving as signaling molecules, protective agents of the immune system, structural constituents, transporters, enzymes, and even as a nutritional source. In biological systems, peptides manifest as short polymers of amino acids connected via peptide bonds - a linkage established between the carboxyl group of one amino acid and the amino group of another. These entities perform a comprehensive array of functions in living organisms. For instance, they function as signaling molecules, safeguarding agents of the immune system, structural components, transporters, and enzymes. Moreover, they also serve as a source of nutrition [66]. Since each amino acid is composed of many heavy atoms, the molecular graph of a peptide is much larger than that of a small drug-like molecule. The long-range molecular benchmark proposes two datasets for Peptides property prediction where the graphs are derived such that the nodes correspond to the heavy (non-hydrogen) atoms of the peptides while the edges represent the bonds that join them. The peptides datasets have about 5 times larger diameter (≈ 57) and 6 times more atoms than the molecular graphs present in the ZINC benchmark (≈ 151) and the average node degree is 2.04. The average shortest path is 20.89. The requirements for long-range interactions and sensitivity to the graph’s global properties are met through the three-dimensional structural dependencies intrinsic to the peptide chains combined with a substantial raise in number of nodes in the graphs.

E.4 TUDataset

The TUDataset [97] is a rich repository of graph-based datasets, serving as a benchmark for learning tasks on graph-structured data. Specifically, we took the ones within the domain of small molecules and bioinformatics. The MUTAG dataset, for instance, comprises nitroaromatic compounds, where the task is to predict their mutagenicity on *Salmonella typhimurium* [98]. The dataset is structured as graphs, with vertices representing atoms labeled by atom type and edges representing bonds between the corresponding atoms, consisting of 188 samples of chemical compounds with 7 discrete node labels. Another dataset used is PTC, a collection of 344 chemical compounds, each represented as a graph, with the goal to report carcinogenicity for rodents, and 19 node labels for each node [99].

The NCI1 and NCI109 and dataset, from the cheminformatics domain, represents each chemical compound as a graph, where vertices and edges respectively symbolize atoms and bonds between atoms. The dataset pertains to anti-cancer screens with chemicals evaluated for their effectiveness against cell lung cancer [100]. Each vertex label denotes the corresponding atom type, encoded via a one-hot-encoding scheme into a binary vector. The PROTEINS dataset is utilized in the field of bioinformatics for protein function prediction [101]. The task is to predict functional class membership of enzymes and non-enzymes. We assess the performance of enhanced topological message passing scheme against graph kernel methods, graph neural networks as well as topological neural networks. In this assessment, we employed the same model configurations used in [14]. In Table 5 we report that the proposed scheme achieves state of the art results on four out of five different evaluations. The exception is for NCI1 where our method achieves the second place after WL kernel [92].